

ARTICLE

Photodissociation and Density Functional Calculations of Small $V_m O_n^+$ Clusters[†]

Ren-zhong Li, Hong-guang Xu, Guo-jin Cao, Yu-chao Zhao, Wei-jun Zheng*

Beijing National Laboratory for Molecular Sciences, State Key Laboratory of Molecular Reaction Dynamics, Institute of Chemistry, Chinese Academy of Sciences, Beijing 100190, China

(Dated: Received on August 15, 2011; Accepted on September 22, 2011)

Oxygen-poor vanadium oxide clusters, $V_2 O_n^+$ ($n=1, 2$), $V_3 O_n^+$ ($n=1, 2, 3$), and $V_4 O_3^+$, were produced by laser vaporization and were mass-selected and photodissociated with 532 and 266 nm photons. The geometric structures and possible dissociation channels of these clusters were determined based on the comparison of density functional calculations and photodissociation experiments. The experiments show that the dissociation of $V_2 O^+$, $V_2 O_2^+$, and $V_3 O_3^+$ mainly occurs by loss of VO, while the dissociation of $V_3 O^+$ and $V_4 O_3^+$ mainly occurs by loss of V atom. For the dissociation of $V_3 O_2^+$, the VO loss channel is slightly dominant compared to the V loss channel. The combination of experimental results and theoretical calculations suggests that the V loss channels of $V_3 O^+$ and $V_4 O_3^+$ are single photon processes at both 532 and 266 nm. The VO loss channels of $V_2 O_2^+$ and $V_3 O_3^+$ are multiple-photon processes at both 532 and 266 nm.

Key words: Mass spectrometry, Mass-selection, Photodissociation, Vanadium oxide cluster

I. INTRODUCTION

Vanadium oxides are of increasing importance in technological applications, such as industrial catalysis [1–4] and optical materials [5]. It is very necessary to investigate the structures and stabilities of vanadium oxide clusters in order to have a better understanding of their reactivity and their role in catalysis. It is noteworthy that a variety of experiments have been performed to study the vanadium oxide clusters [6–16]. Bernstein and coworkers have studied the growth dynamics and structures of neutral vanadium oxide clusters with ultraviolet laser photoionization and density functional calculations [7–9]. Castleman and coworkers have investigated the reactivity of vanadium oxide clusters with small hydrocarbons [11–14, 16]. Duncan and coworkers have conducted photodissociation experiments on $V_n O_m^+$ ($m > n$) clusters [15]. Infrared spectroscopy [17, 18] and photoelectron spectroscopy [19–23] have also been employed to investigate the vibrational and electronic properties of vanadium oxides. As for the theoretical studies, the structures, stabilities, and electronic states of vanadium oxide clusters were investigated with density functional calculations by many research groups [14, 24–30]. Despite of the abundance

of experimental and theoretical work on vanadium oxides, the study on oxygen-deficient vanadium oxide clusters is very rare. Systematic behavior of vanadium oxide clusters is not completely understood. In this work, we combine the laser photodissociation experiment with density functional calculations to study the structures of several small oxygen-poor vanadium oxide clusters, $V_2 O_n^+$ ($n=1, 2$), $V_3 O_n^+$ ($n=1, 2, 3$), and $V_4 O_3^+$.

II. EXPERIMENTAL AND COMPUTATIONAL METHODS**A. Experiments**

The experiments were conducted on a home-built reflectron time-of-flight mass spectrometer, which has been described elsewhere [31]. Briefly, vanadium-oxide clusters were generated in a laser vaporization source, where a rotating and translating V/V₂O₅ disc target (13 mm diameter, V/V₂O₅ mole ratio 10:1) was ablated with the second harmonic (532 nm) light pulses of a Nd:YAG laser, while helium gas with 400 kPa backing pressure was allowed to expand through a pulsed valve over the target. The laser fluence for laser ablation was about 25 GW/cm². The vanadium-oxide clusters were then mass-analyzed with the reflectron time-of-flight mass spectrometer. For the photodissociation experiments, we used a deceleration-dissociation-reacceleration method. The cluster ions of interests were selected with a mass gate at the first space focus region of the reflectron time-of-flight mass spectrometer, were decelerated with deceleration plates right af-

[†]Part of the special issue for “the Chinese Chemical Society’s 12th National Chemical Dynamics Symposium”.

* Author to whom correspondence should be addressed. E-mail: zhengwj@iccas.ac.cn, Tel.: +86-10-62635054, FAX: +86-10-62563167

ter the mass gate, and were photodissociated with a nanosecond Nd:YAG laser (Continuum Surelite II-10) at 532 and 266 nm wavelengths. The fragment ions and surviving parent ions were re-accelerated toward the reflectron plates, then reflected to the MCP (microchannel plates) detector of the mass spectrometer. The mass signals were amplified with a broadband amplifier, were digitized with a 100 MHz digit card, and were collected in a laboratory computer with a home-made software.

B. Computational method

All calculations were performed with the density functional theory (DFT) using the hybrid B3LYP [32–35] exchange-correlation functional as implemented in the Gaussian 09 [36] program package. 6-311G(d) basis set was employed for all calculations. Geometric configurations of $V_2O_n^+$ ($n=1, 2$), $V_3O_n^+$ ($n=1, 2, 3$), and $V_4O_3^+$ were fully optimized. Several stable equilibrium isomers were obtained. In order to verify that those isomers are real local minima on potential surfaces, vibration frequency calculations were also performed at all optimized geometric structures. Those geometric structures have been confirmed to have no imaginary frequency. The bond dissociation energies (BDEs) and natural atomic orbital (NAO) analysis of these vanadium oxides were also examined to further investigate the bonding properties and the spin densities on the atoms.

III. EXPERIMENTAL RESULTS

Figure 1 shows a typical, reproducible mass spectrum of the $V_mO_n^+$ cluster ions generated in the experiments. Here the major mass peaks in the spectrum are those of $V_mO_n^+$ cluster ions with m and n smaller than 5.

To investigate the relative stabilities of these clusters, we performed mass-selected photodissociation experiments of $V_2O_n^+$ ($n=1, 2$), $V_3O_n^+$ ($n=1, 2, 3$), and $V_4O_3^+$ by 532 and 266 nm photons. Figure 2 shows the typical photodissociation mass spectra of the vanadium oxide cluster ions. The photodissociation experiments were conducted with the photodissociation laser on and off alternatively shot by shot. The photodissociation mass spectra were obtained by subtracting the data taken with the photodissociation laser off from the data with the photodissociation laser on. The upward peaks are the mass peaks of the fragment ions, while the downward peaks are the depletion of the parent ions. The photodissociation efficiencies of the fragment ions are summarized in Table I. The photodissociation efficiency of each fragment ion was calculated with Eq.(1):

$$R_j = \frac{I_j}{\sum I_i} \quad (1)$$

where I_j is the intensity of the studied fragment ion,

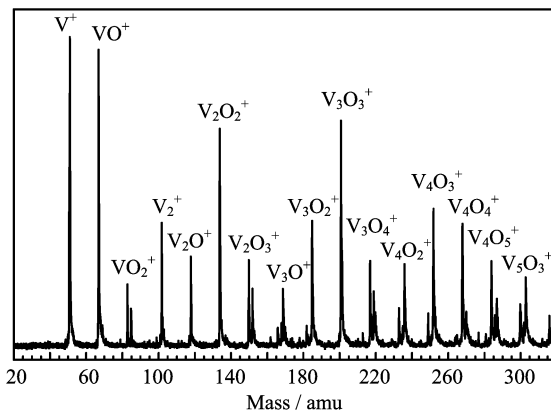


FIG. 1 Mass spectrum of $V_xO_y^+$ cluster ions.

and $\sum I_i$ is the total intensity of the fragment ions and remaining parent ions.

From Fig.2, we can see that V^+ is the main fragment ion for the dissociation of V_2O^+ . At 532 nm, V_2O^+ yields only V^+ fragment ion by loss of VO . At 266 nm, however, two photofragment ions, V^+ and VO^+ , are generated by eliminating VO and V from the V_2O^+ parent ion, respectively.

Dissociation of $V_2O_2^+$ mainly generates VO^+ fragment ion and tiny amount of V^+ fragment ion at 532 nm. The dissociation behavior of the $V_2O_2^+$ at 266 nm is similar to that at 532 nm, except that the dissociation efficiency at 266 nm is higher than that at 532 nm.

Dissociation of V_3O^+ at 532 nm yields mostly V_2O^+ fragment ion and tiny amount of V_2^+ and V^+ . In this case, the V_2O^+ fragment ion corresponds to the loss of V neutral. Dissociation of V_3O^+ at 266 nm produces four fragment ions, V^+ , VO^+ , V_2^+ and V_2O^+ . From Fig.2(c) and Table I, we can see that the main fragment ions of V_3O^+ at 266 nm are V_2O^+ and V^+ . It is noteworthy that the VO^+ fragment ion is not observed at 532 nm. Compared to the dissociation behavior of V_2O^+ at 266 nm, we can infer that the VO^+ fragment ion is produced by a sequential dissociation process $V_3O^+ \rightarrow V_2O^+ \rightarrow VO^+$ at 266 nm. In addition, the branching ratio of V^+ fragment ion at 266 nm is much higher than that at 532 nm. We speculated that the V^+ fragment ion could also come as a sequential product from further dissociation of V_2O^+ fragment ion at 266 nm.

For the dissociation of $V_3O_2^+$ at 532 nm, $V_2O_2^+$ and V_2O^+ fragment ions are detected at low photon flux (Fig.2(a)), and an additional fragment ion V^+ can be observed at higher photon flux (Fig.2(b)). As for the dissociation of $V_3O_2^+$ at 266 nm, the VO^+ fragment ion is also observed in addition to the $V_2O_2^+$ and V_2O^+ fragment ions. The VO^+ fragment ion of $V_3O_2^+$ probably is generated from V_2O loss channel ($V_3O_2^+ \rightarrow V_2O + VO^+$) or is formed by stepwise

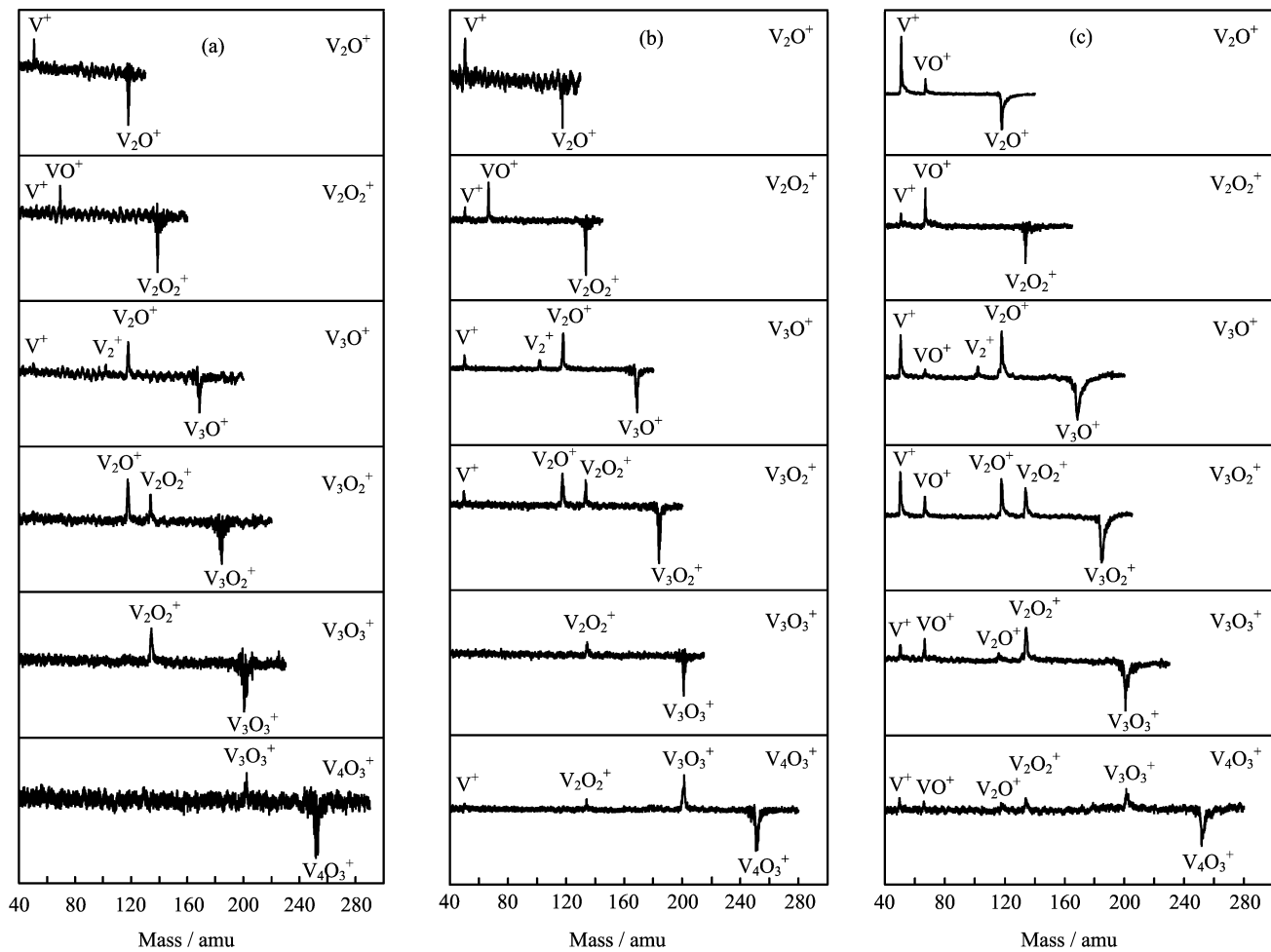


FIG. 2 Photodissociation mass spectra of V_2O_n^+ ($n=1, 2$), V_3O_n^+ ($n=1, 2, 3$), and V_4O_3^+ . (a) At 532 nm with laser power of 7 MW/cm², (b) at 532 nm with laser power of 14 MW/cm², (c) at 266 nm with laser power of 7 MW/cm².

dissociation path ($\text{V}_3\text{O}_2^+\rightarrow\text{V}_2\text{O}^+\rightarrow\text{VO}^+$). Also, for the dissociation of V_3O_2^+ , the branching ratio of V^+ fragment ion at 266 nm is much higher than that at 532 nm. We infer that both V_2O_2 elimination channel ($\text{V}_3\text{O}_2^+\rightarrow\text{V}_2\text{O}_2+\text{V}^+$) and sequential dissociation path ($\text{V}_3\text{O}_2^+\rightarrow\text{V}_2\text{O}^+\rightarrow\text{V}^+$) contribute to the generation of V^+ fragment ion.

As for the dissociation of V_3O_3^+ at 532 nm, there is only V_2O_2^+ fragment ion by loss of VO . But, four fragment ions, V_2O_2^+ , V_2O^+ , VO^+ , and V^+ , are observed at 266 nm. V_2O_2^+ is the major fragment ion at both 532 and 266 nm.

The dissociation of V_4O_3^+ at 532 nm with low photon flux (Fig.2(a)) produces V_3O_3^+ fragment ion, V_2O_2^+ and V^+ fragment ions can also be observed with higher photon flux (Fig.2(b)). At 266 nm, the dissociation of V_4O_3^+ yields five fragments V_3O_3^+ , V_2O_2^+ , V_2O^+ , VO^+ , and V^+ . V_3O_3^+ is the major fragment ion at both 532 and 266 nm. It is obvious that the V_3O_3^+ fragment ion is generated by loss of V atom ($\text{V}_4\text{O}_3^+\rightarrow\text{V}+\text{V}_3\text{O}_3^+$), while the production of V_2O_2^+ could occur by the loss of V_2O di-

rectly ($\text{V}_4\text{O}_3^+\rightarrow\text{V}_2\text{O}+\text{V}_2\text{O}_2^+$) or by the sequential dissociation path $\text{V}_4\text{O}_3^+\rightarrow\text{V}_3\text{O}_3^+\rightarrow\text{V}_2\text{O}_2^+$. Likewise, the production of VO^+ could occur by V_3O_2 loss channel ($\text{V}_4\text{O}_3^+\rightarrow\text{V}_3\text{O}_2+\text{VO}^+$), and that of V^+ by V_3O_3 loss channel ($\text{V}_4\text{O}_3^+\rightarrow\text{V}^+$). VO^+ and V^+ might also be produced from sequential dissociation channels.

Overall, the photodissociation experiments show that the dissociation of V_2O^+ , V_2O_2^+ , and V_3O_3^+ mainly occurs by loss of VO , while the dissociation of V_3O^+ and V_4O_3^+ mainly occurs by loss of V atom. For the dissociation of V_3O_2^+ , the branch ratios of the VO loss channel and V loss channel are similar to the VO loss channel slightly dominant.

IV. THEORETICAL RESULTS AND DISCUSSION

The optimized geometries of the low-lying isomers of V_xO_y^+ clusters obtained with DFT calculations are presented in Fig.3 with the most stable structures on the left. In order to examine the relative stabilities and photodissociation mechanisms of V_2O_n^+ ($n=1, 2$), V_3O_n^+

TABLE I Dissociation channels, bond dissociation energies, and photodissociation efficiencies of the most stable isomers of $V_2O_n^+$ ($n=1, 2$), $V_3O_n^+$ ($n=1, 2, 3$), and $V_4O_3^+$ clusters. R_{j1} and R_{j2} correspond to the dissociation at 532 nm with laser power of 7 and 14 MW/cm² respectively; R_{j3} corresponds to the dissociation at 266 nm with laser power of 7 MW/cm².

Cluster		Dissociation channel	BDE/eV	R_{j1}	R_{j2}	R_{j3}
$V_2O^+(^8A')$	1A	(1a) $VO + V^+$	3.42	0.053	0.127	0.399
		(1b) $V + VO^+$	4.58			0.099
$V_2O_2^+(^6A')$	2A	(2a) $VO + VO^+$	5.05	0.051	0.093	0.086
		(2b) $VO_2 + V^+$	6.31		0.032	0.025
$V_3O^+(^{11}A)$	3A	(3a) $V + V_2O^+$	2.36	0.153	0.204	0.229
		(3b) $VO + V_2^+$	3.95	0.049	0.056	0.052
		(3c) $V_2O + V^+$	3.81		0.078	0.205
		(3d) $V_2 + VO^+$	6.38			0.043
$V_3O_2^+(^5A'')$	4A	(4a) $V + V_2O_2^+$	4.56	0.071	0.123	0.100
		(4b) $VO + V_2O^+$	3.40	0.101	0.156	0.135
		(4c) $V_2O_2 + V^+$	4.60		0.063	0.159
		(4d) $V_2O + VO^+$	7.01			0.066
$V_3O_3^+(^3B_1)$	5A	(5a) $VO + V_2O_2^+$	5.12	0.038	0.061	0.085
		(5b) $VO_2 + V_2O^+$	5.63			0.019
		(5c) $V_2O_2 + VO^+$	7.70			0.050
		(5d) $V_2O_3 + V^+$	6.14			0.035
$V_4O_3^+(^6A)$	6A	(6a) $V + V_3O_3^+$	2.25	0.088	0.163	0.178
		(6b) $V_2O + V_2O_2^+$	6.88		0.053	0.114
		(6c) $V_3O_3 + V^+$	4.63		0.026	0.093
		(6d) $V_2O_2 + V_2O^+$	6.87			0.063
		(6e) $V_3O_2^+ + VO^+$	7.54			0.081

($n=1, 2, 3$), and $V_4O_3^+$, we calculated their bond dissociation energies (BDEs) based on the energies of their most stable structures. The BDEs are evaluated as the differences of the total energy of the parent ions and the sum of the energies of the fragments. The calculated BDEs of the most stable clusters are presented in Table I.

The most stable structure of V_2O^+ is isomer 1A in ${}^8A'$ state with C_s symmetry. It is a quasi-linear structure with the O atom bridging the two V atoms, quite similar to the structure of AlVO [37]. In isomer 1A, one of the V1–O bond is longer than the V2–O bond. In order to investigate the bond properties of the $V_mO_n^+$ clusters, we conducted Wiberg bond order analysis using the NBO 3.1 program [38] implemented in the Gaussian 09 software package. The bond order analysis shows that the bond order values of V1–O and V2–O are 0.41 and 1.26, respectively. V1–O can be considered as a single bond while V2–O bond is between the single and double bond. Thus, the most probable dissociation channel of V_2O^+ is by loss of VO to produce V^+ . Our calculations (Table I) show that it takes about 3.42 eV for isomer 1A to be dissociated into $VO + V^+$ (channel (1a)), and about 4.58 eV for it to be dissociated into $V + VO^+$ (channel (1b)). The V^+ fragment ion observed at 532 nm in the experiments probably is from two-photon process since the dissociation energy of channel (1a) is higher than the photon energy

of a 532 nm photon. A 266 nm photon is able to initiate dissociation through both channel (1a) and (1b). The calculated structure and dissociation channels of isomer 1A are in good agreement with the photodissociation experiments. Isomers 1B, 1C, and 1D are much higher than isomer 1A in energy, they are unlikely to be populated in our experiments. We suggest that isomer 1A is the most probable structure observed in our experiment.

The lowest energy structure of $V_2O_2^+$ is isomer 2A in ${}^6A'$ state with C_s symmetry. It is a VOVO four-membered ring. Regarding the ground state of $V_2O_2^+$, there are some disagreements in the literature. Calatayud *et al.* calculated the ground state of $V_2O_2^+$ to be ${}^2A'$ [27], while Jakubikova *et al.* reported the ground state of $V_2O_2^+$ to be a sextet state [30]. Our calculations are in agreement with that Jakubikova *et al.* [30]. Wiberg bond order analysis shows that the bond order values of V1–O1, V1–O2, V2–O1, and V2–O2 bonds are 0.73, 0.40, 0.93, and 1.40, respectively. Thus, V1–O1, V2–O1, and V1–O2 can be considered as single bond, while V2–O2 is between the single and double bond. The dissociation of $V_2O_2^+$ can occur by first break the V1–O2 bond, then break the V2–O1 bond, therefore, generates $VO + VO^+$. The dissociation can also occur by breaking the V1–O2 and V1–O2 bonds to generate $VO_2 + V^+$. These are consistent with VO^+ and V^+ fragment ions observed in the

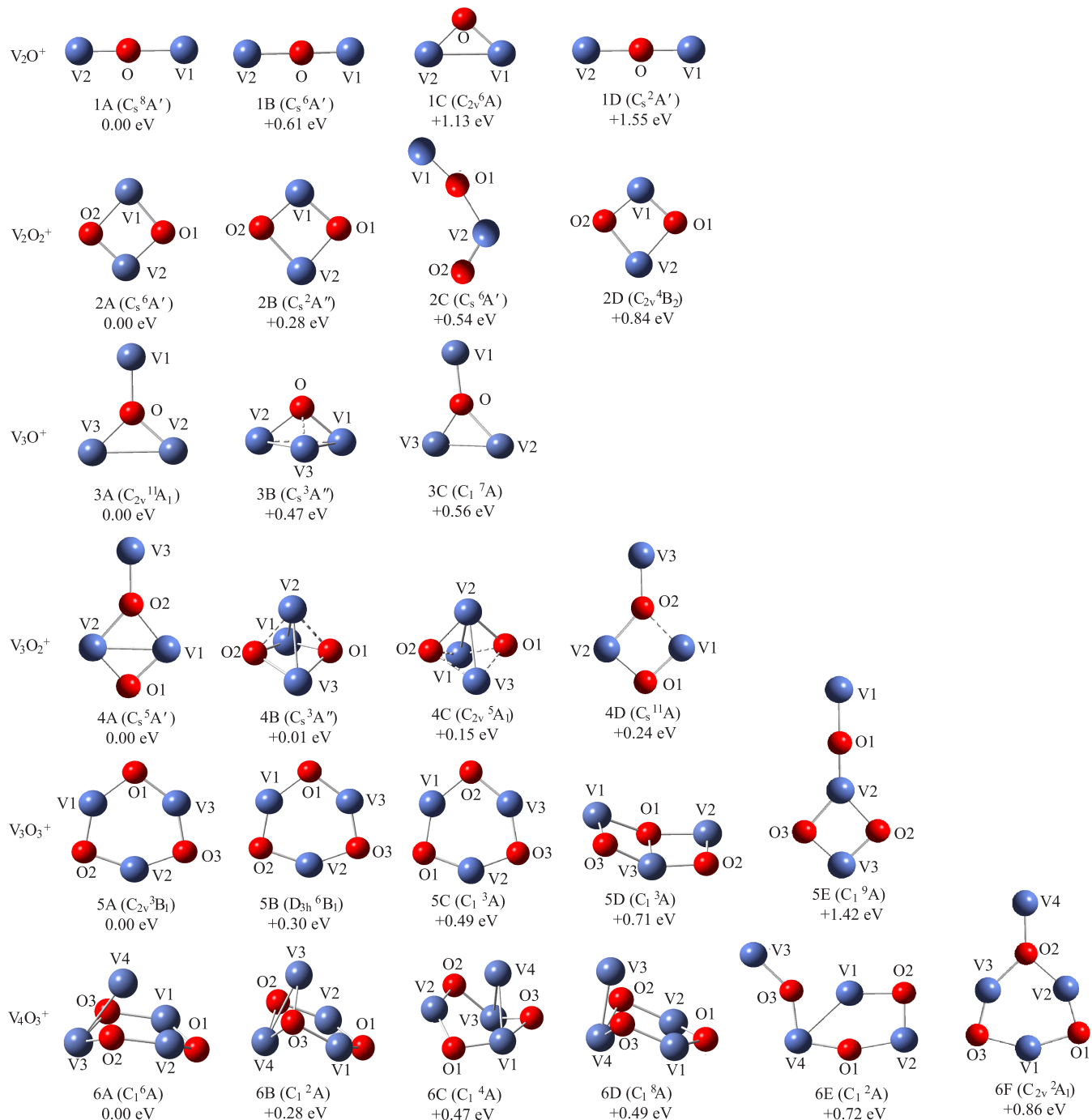


FIG. 3 Structures of the typical low-lying isomers of $V_2O_n^+$ ($n=1, 2$), $V_3O_n^+$ ($n=1, 2, 3$), and $V_4O_3^+$. The energies relative to the most stable isomer are shown under them.

experiments. As can be seen in Table I, the BDEs of channels (2a) and (2b) are calculated to be 5.01 and 6.31 eV, respectively. The BDEs are higher than the photon energies of 532 and 266 nm photons. Therefore, we suggest that channels (2a) and (2b) are multiphoton processes at both 532 and 266 nm. Three 532 nm photons or two 266 nm photons are needed to dissociation $V_2O_2^+$. That is in agreement with the low dissociation

efficiencies of $V_2O_2^+$ in the experiments. The structure of isomer 2B is very similar to that of isomer 2A. It is higher than isomer 2A by 0.28 eV and can be considered as an electronic excited state of isomer 2A. Isomers 2C and 2D are much higher in energy than isomer 2A. We suggest that it is unlikely for isomers 2B, 2C, and 2D to exist in the experiments.

The most stable structure of $V_3O_1^+$ is isomer 3A in

TABLE II Natural charge and spin density distributions of the most stable isomers of $V_2O_n^+$ ($n=1, 2$), $V_3O_n^+$ ($n=1, 2, 3$), and $V_4O_3^+$ clusters.

Cluster	Atom	Natural electron configuration	Natural charge	Spin density
$V_2O^+({}^8A')$	V1	[core]4s ^{0.73} 3d ^{3.35}	0.92	3.90
	V2	[core]4s ^{0.58} 3d ^{3.38}	1.06	3.40
	O	[core]2s ^{1.89} 2p ^{5.08}	-0.97	0.29
$V_2O_2^+({}^6A')$	V1	[core]4s ^{0.21} 3d ^{3.42}	1.37	3.01
	V2	[core]4s ^{0.32} 3d ^{3.31}	1.38	2.24
	O1	[core]2s ^{1.91} 2p ^{5.00}	-0.92	-0.09
	O2	[core]2s ^{1.91} 2p ^{4.91}	-0.82	-0.15
$V_3O^+({}^{11}A)$	V1	[core]4s ^{0.77} 3d ^{3.43}	0.80	3.98
	V2	[core]4s ^{0.87} 3d ^{3.41}	0.72	3.07
	V3	[core]4s ^{0.87} 3d ^{3.41}	0.72	3.07
	O	[core]2s ^{1.90} 2p ^{5.34}	-1.24	-0.13
$V_3O_2^+({}^5A'')$	V1	[core]4s ^{0.44} 3d ^{3.37}	1.18	-2.88
	V2	[core]4s ^{0.32} 3d ^{3.42}	1.26	2.94
	V3	[core]4s ^{1.03} 3d ^{3.25}	0.72	4.01
	O1	[core]2s ^{1.91} 2p ^{5.02}	-0.94	-0.00
	O2	[core]2s ^{1.89} 2p ^{5.34}	-1.23	-0.07
$V_3O_3^+({}^3B_1)$	V1	[core]4s ^{0.32} 3d ^{3.37}	1.30	2.33
	V2	[core]4s ^{0.39} 3d ^{3.37}	1.24	-2.57
	V3	[core]4s ^{0.32} 3d ^{3.37}	1.31	2.33
	O1	[core]2s ^{1.89} 2p ^{5.06}	-0.95	-0.10
	O2	[core]2s ^{1.89} 2p ^{5.05}	-0.95	0.00
	O3	[core]2s ^{1.89} 2p ^{5.05}	-0.95	0.00
$V_4O_3^+({}^6A)$	V1	[core]4s ^{0.48} 3d ^{3.44}	1.08	2.72
	V2	[core]4s ^{0.48} 3d ^{3.44}	1.09	2.73
	V3	[core]4s ^{0.35} 3d ^{3.42}	1.23	2.84
	V4	[core]4s ^{0.59} 3d ^{3.63}	0.78	-3.07
	O1	[core]2s ^{1.88} 2p ^{5.05}	-0.94	-0.15
	O2	[core]2s ^{1.89} 2p ^{5.22}	-1.12	-0.03
	O3	[core]2s ^{1.89} 2p ^{5.22}	-1.12	-0.03

${}^{11}A_1$ state with C_{2v} symmetry. It has a V atom weakly bound to the O atom of the V_2O triangle. Wiberg bond order analysis shows that the bond orders for $V2-O$, $V3-O$, and $V2-V3$ bonds are 0.49, 0.49, and 0.94, respectively, indicating that these bonds are all single bonds. The calculated $V1-O$ bond order value is only 0.34, indicating that the dissociation of V_3O^+ can occur by breaking the $V1-O$ bond to produce $V+V_2O^+$ or V_2O+V^+ , corresponding to the observation of V_2O^+ and V^+ fragment ions in the experiments. The V_2^+ and VO^+ fragment ions probably can be formed by breaking the $V2-O$ and $V3-O$ bonds together. The VO^+ fragment ion observed at 266 nm can also come from further dissociation of V_2O^+ fragment. Our calculations show that BDEs of channel (3a) and (3c) are 2.36 and 3.81 eV, respectively. The calculated BDE of channel (3a) (2.36 eV) is very close to the photon energy of a 532 nm photon. Considering the uncertainty of theoretical calculations, we suggest that the actually BDE of channel (3a) might be lower than the photon energy

of a 532 nm photon. Thus, channel (3a) probably only requires one 532 nm photon, while channel (3c) requires two 532 nm photons. That probably can explain why the branch ratio of V_2O^+ fragment ion is higher than that of V^+ at 532 nm in the experiments. Either channel (3a) or (3c) needs only one 266 nm photon. That can explain why the branch ratios of V_2O^+ and V^+ are similar at 266 nm (Fig.2). Isomers 3B and 3C are 0.47 and 0.56 eV higher in energy than isomer 3A, respectively. They probably are not present in the experiments.

The first two isomers of $V_3O_2^+$ (4A and 4B) are nearly degenerate in energy with 4B higher than 4A by only 0.01 eV. Isomer 4A has a V atom attaching to the one of the O atoms in the OVOV four-membered ring. Isomer 4B has a V atom over the OVOV four-membered ring. Therefore, both isomers 4A and 4B probably exist in our experiments. The energy of isomers 4C and 4D are much higher than isomer 4A and 4B, thus, they probably do not exist in the experiments. For isomer 4A, the calculated bond order values are in

the range of 0.37–0.85. All of them can be considered as single bonds. The calculated BDEs of channel (4a), (4b), and (4c) are 4.56, 3.40, and 4.60 eV, respectively. These dissociation channels are two-photon processes at 532 nm and one photon processes at 266 nm. These are consistent with the observation of $V_2O_2^+$, V_2O^+ , and V^+ fragment ions in the experiment. The calculated BDE of channel (4d) is about 7.01 eV, higher than the total energy of two 532 nm photons and lower than the total energy of two 266 nm photons. Thus, the VO⁺ fragment ion is detected at 266 nm but is not detected at 532 nm.

The most stable structure of $V_3O_3^+$ is isomer 5A in 3B_1 state with C_{2v} symmetry. It is a six-membered ring structure. The geometric structures of isomer 5B and 5C are very similar to that of isomer 5A except that they are in different electronic states. Isomers 5B and 5C can be considered as the electronic excited states of isomer 5A. Since the energy of isomers 5B, 5C, 5D, and 5E are much higher, isomer 5A is the most probable structure observed in our experiments. Wiberg bond order analysis shows that the V–O bond order values of isomer 5A are in the range of 0.74–0.86, indicating these V–O bonds are all typical single bonds. At least two bonds need to be broken in order to dissociate isomer 5A since it is a ring structure. The calculated BDEs of channels (5a), (5b), (5c), and (5d) are 5.13, 5.63, 7.70, and 6.14 eV, respectively. They are higher than the energy of two 532 nm photons or one 266 nm photon. That indicates that the $V_2O_2^+$ fragment ion is generated by three-photon process at 532 nm and two-photon process at 266 nm. That is in agreement with our experimental observation since the dissociation efficiency of $V_3O_3^+$ is relatively low.

The most stable structure of $V_4O_3^+$ is isomer 6A in 6A state. It has a vanadium atom attaching to the distorted V_3O_3 six-membered ring through one of the vanadium atoms in the ring. As isomers 6B, 6C, 6D, 6E, and 6F are 0.28–0.86 eV higher than isomer 6A in energy, they probably are not present in the experiments. Here we only discuss isomer 6A in detail. The bond order analysis of isomer 6A show that the bond order value of V4–V3 bond is only 0.39, indicating that it can be broken easily. The other V–O bond order values are in the range of 0.50–0.82, we can regard these bonds as single bonds. As for dissociation behavior of isomer 6A, the main dissociation channel is to produce $V_3O_3^+$ by losing V at both 532 and 266 nm. The BDE of the V loss channel (6a) is calculated to be 2.25 eV, smaller than the photon energy of a 532 or 266 nm photon. Therefore, the production of $V_3O_3^+$ fragment ion by V loss is single photon process at both 532 and 266 nm. The other dissociation channels probably are multiphoton processes. Some of the fragment ions, such as $V_2O_2^+$, V_2O^+ , VO^+ , and V^+ , may also be contributed by sequential dissociation paths.

Generally, the geometric structures and BDEs from theoretical calculations are in good agreement with the

experimental phenomena. It is confirmed by both experiments and theoretical calculations that the V loss channels of $V_3O_3^+$ and $V_4O_3^+$ are single photon processes at both 532 and 266 nm. The VO loss channels of $V_2O_2^+$ and $V_3O_3^+$ are multiple-photon processes at both 532 and 266 nm. For the other dissociation channels of these $V_mO_n^+$ clusters, we find that high photon flux is necessary to achieve significant amount of dissociation at 532 nm. That indicates that these dissociations are mostly multiphoton processes at 532 nm, consistent with the BDEs from the density functional calculations. Duncan and coworkers have investigated the photodissociation processes of oxygen-abundant $V_mO_n^+$ ($n > m$) clusters at 355 and 532 nm and found that multiphoton processes are required [15]. The multiphoton dissociation channels observed in the study of the oxygen-poor $V_mO_n^+$ ($n < m$) clusters are in agreement with their findings.

Table II presents the atomic natural electron configuration and the atomic spin densities for the most stable isomers of $V_mO_n^+$ clusters. It can be seen that the vanadium atoms always possess positive charges in the range of 0.92e–1.38e while the oxygen atoms have negative charges from –0.82e to –1.24e.

Regarding the spin densities, an obvious trend is observed. The spin densities localize exclusively on vanadium centers for the oxygen-poor vanadium oxide clusters which means the unpaired electrons mainly localize on the vanadium 3d orbitals. Thus, vanadium atoms have the highest values of spin density in general. Considering the electronic states of the most stable structures of $V_mO_n^+$ clusters, V_2O^+ (${}^8A'$), $V_2O_2^+$ (${}^6A'$), V_3O^+ (${}^{11}A_1$), $V_3O_2^+$ (${}^5A''$), $V_3O_3^+$ (3B_1), and $V_4O_3^+$ (6A), we can see that the oxygen-deficient clusters tend to have higher spin states. That is in accordance with the higher spin densities on the vanadium atoms.

V. CONCLUSION

Oxygen-poor vanadium oxide clusters, $V_2O_n^+$ ($n=1, 2$), $V_3O_n^+$ ($n=1, 2, 3$), and $V_4O_3^+$, were studied using photodissociation experiments and density functional calculations. The experiments show that the dissociation of V_2O^+ , $V_2O_2^+$, and $V_3O_3^+$ mainly occurs by loss of VO, while the dissociation of V_3O^+ and $V_4O_3^+$ mainly occurs by loss of V atom. For the dissociation of $V_3O_2^+$, the VO loss channel is slightly dominant compared to the V loss channel. The geometric structures and possible dissociation channels of these clusters were determined based on the comparison of density functional calculations and photodissociation experiments. The combination of experimental results and theoretical calculations suggests that the V loss channels of $V_3O_3^+$ and $V_4O_3^+$ are single photon processes at both 532 and 266 nm. The VO loss channels of $V_2O_2^+$ and $V_3O_3^+$ are multiple-photon processes at both 532 and 266 nm.

VI. ACKNOWLEDGMENTS

This work was supported by the National Natural Science Foundation of China (No.20933008). The theoretical calculations were conducted on the ScGrid and Deepcomp7000 of the Supercomputing Center, Computer Network Information Center of Chinese Academy of Sciences. We thank Dr. Xun-lei Ding and Dr. Yan-xia Zhao for valuable discussion.

- [1] I. M. Campbell, *Catalysis at Surfaces*, New York: Chapman and Hall Ltd., (1988).
- [2] P. A. Cox, *Transition Metal Oxides*, Oxford: Clarendon Press, (1992).
- [3] N. Y. Topsoe, *Science* **265**, 1217 (1994).
- [4] C. N. R. Rao and B. Rave, Ed., *Transition Metal Oxides: Structure, Properties, and Synthesis of Ceramic Oxides*, New York: John Wiley, (1998).
- [5] C. E. Lee, R. A. Atkins, W. N. Gibler, and H. F. Taylor, *Appl. Opt.* **28**, 4511 (1989).
- [6] J. Xu, M. T. Rodgers, J. B. Griffin, and P. B. Armentrout, *J. Chem. Phys.* **108**, 9339 (1998).
- [7] M. Foltin, G. J. Stueber, and E. R. Bernstein, *J. Chem. Phys.* **111**, 9577 (1999).
- [8] Y. Matsuda and E. R. Bernstein, *J. Phys. Chem. A* **109**, 3803 (2005).
- [9] F. Dong, S. Heinbuch, S. G. He, Y. Xie, J. J. Rocca, and E. R. Bernstein, *J. Chem. Phys.* **125**, 164318 (2006).
- [10] R. C. Bell, K. A. Zemski, K. P. Kerns, H. T. Deng, and A. W. Castleman, *J. Phys. Chem. A* **102**, 1733 (1998).
- [11] S. E. Kooi and A. W. Castleman, *J. Phys. Chem. A* **103**, 5671 (1999).
- [12] R. Bell, K. Zemski, D. Justes, and A. Castleman Jr., *J. Chem. Phys.* **114**, 798 (2001).
- [13] K. A. Zemski, D. R. Justes, and A. W. Castleman, *J. Phys. Chem. B* **106**, 6136 (2002).
- [14] D. R. Justes, R. Mitić, N. A. Moore, V. Bonačić-Koutecký, and A. W. Castleman, *J. Am. Chem. Soc.* **125**, 6289 (2003).
- [15] K. S. Molek, T. D. Jaeger, and M. A. Duncan, *J. Chem. Phys.* **123**, 144313 (2005).
- [16] D. R. Justes, N. A. Moore, and A. W. Castleman, *J. Phys. Chem. B* **108**, 3855 (2004).
- [17] K. R. Asmis, G. Meijer, M. Brummer, C. Kaposta, G. Santambrogio, L. Woste, and J. Sauer, *J. Chem. Phys.* **120**, 6461 (2004).
- [18] K. R. Asmis, G. Santambrogio, M. Brummer, and J. Sauer, *Angew. Chem. Int. Edit.* **44**, 3122 (2005).
- [19] C. S. Feigerle, R. R. Corderman, S. V. Bobashev, and W. C. Lineberger, *J. Chem. Phys.* **74**, 1580 (1981).
- [20] H. Wu and L. S. Wang, *J. Chem. Phys.* **108**, 5310 (1998).
- [21] S. M. E. Green, S. Alex, N. L. Fleischer, E. L. Millam, T. P. Marcy, and D. G. Leopold, *J. Chem. Phys.* **114**, 2653 (2001).
- [22] H. J. Zhai and L. S. Wang, *J. Chem. Phys.* **117**, 7882 (2002).
- [23] A. Pramann, K. Koyasu, A. Nakajima, and K. Kaya, *J. Chem. Phys.* **116**, 6521 (2002).
- [24] M. Calatayud, J. Andrés, A. Beltrán, and B. Silvi, *Theor. Chem. Acc.* **105**, 299 (2001).
- [25] S. F. Vyboishchikov and J. Sauer, *J. Phys. Chem. A* **104**, 10913 (2000).
- [26] S. F. Vyboishchikov and J. Sauer, *J. Phys. Chem. A* **105**, 8588 (2001).
- [27] M. Calatayud, J. Andres, and A. Beltran, *J. Phys. Chem. A* **105**, 9760 (2001).
- [28] M. Calatayud, B. Silvi, J. Andéis, and A. Beltrán, *Chem. Phys. Lett.* **333**, 493 (2001).
- [29] J. Sauer and J. Dobler, *Dalton Trans.* 3116 (2004).
- [30] E. Jakubikova, A. K. Rappé, and E. R. Bernstein, *J. Phys. Chem. A* **111**, 12938 (2007).
- [31] Y. C. Zhao, Z. G. Zhang, J. Y. Yuan, H. G. Xu, and W. J. Zheng, *Chin. J. Chem. Phys.* **22**, 655 (2009).
- [32] A. D. Becke, *Phys. Rev. A* **38**, 3098 (1988).
- [33] A. D. Becke, *J. Chem. Phys.* **98**, 5648 (1993).
- [34] C. Lee, W. Yang, and R. G. Parr, *Phys. Rev. B* **37**, 785 (1988).
- [35] P. J. Stephens, F. J. Devlin, C. F. Chabalowski, and M. J. Frisch, *J. Phys. Chem. A* **98**, 11623 (1994).
- [36] M. J. Frisch, G. W. Trucks, H. B. Schlegel, G. E. Scuseria, M. A. Robb, J. R. Cheeseman, G. Scalmani, V. Barone, B. Mennucci, G. A. Petersson, H. Nakatsuji, M. Caricato, X. Li, H. P. Hratchian, A. F. Izmaylov, J. Bloino, G. Zheng, J. L. Sonnenberg, M. Hada, M. Ehara, K. Toyota, R. Fukuda, J. Hasegawa, M. Ishida, T. Nakajima, Y. Honda, O. Kitao, H. Nakai, T. Vreven, J. A. Montgomery, Jr., J. E. Peralta, F. Ogliaro, M. Bearpark, J. J. Heyd, E. Brothers, K. N. Kudin, V. N. Staroverov, R. Kobayashi, J. Normand, K. Raghavachari, A. Rendell, J. C. Burant, S. S. Iyengar, J. Tomasi, M. Cossi, N. Rega, J. M. Millam, M. Klene, J. E. Knox, J. B. Cross, V. Bakken, C. Adamo, J. Jaramillo, R. Gomperts, R. E. Stratmann, O. Yazyev, A. J. Austin, R. Cammi, C. Pomelli, J. W. Ochterski, R. L. Martin, K. Morokuma, V. G. Zakrzewski, G. A. Voth, P. Salvador, J. J. Dannenberg, S. Dapprich, A. D. Daniels, Ö. Farkas, J. B. Foresman, J. V. Ortiz, J. Cioslowski, and D. J. Fox, *Gaussian 09, Revision A.1*, Wallingford CT: Gaussian Inc., (2009).
- [37] Z. G. Zhang, H. G. Xu, X. Y. Kong, and W. J. Zheng, *J. Phys. Chem. A* **115**, 13 (2010).
- [38] E. D. Glendening, A. E. Reed, J. E. Carpenter, and F. Weinhold, NBO Version 3.1.